

Role of Interaction Anisotropy in the Formation and Stability of Molecular Templates

U. K. Weber,¹ V. M. Burlakov,^{1,2} L. M. A. Perdigão,⁴ R. H. J. Fawcett,⁴ P. H. Beton,⁴ N. R. Champness,⁵ J. H. Jefferson,³
G. A. D. Briggs,¹ and D. G. Pettifor¹

¹*Department of Materials, University of Oxford, Parks Road, Oxford OX1 3PH, United Kingdom*

²*Institute for Spectroscopy Russian Academy of Sciences, Troitsk 142190, Russia*

³*QinetiQ, St. Andrews Road, Malvern, WR14 3PS, United Kingdom*

⁴*Schools of Physics and Astronomy, University of Nottingham, University Park, Nottingham NG7 2RD, United Kingdom*

⁵*Schools of Physics Chemistry, University of Nottingham, University Park, Nottingham NG7 2RD, United Kingdom*

(Received 7 September 2007; revised manuscript received 24 January 2008; published 14 April 2008)

Surface templating via self-assembly of hydrogen-bonded molecular networks is a rapidly developing bottom-up approach in nanotechnology. Using the melamine-PTCDI molecular system as an example we show theoretically that the network stability in the parameter space of temperature versus molecular coupling anisotropy is highly restricted. Our kinetic Monte Carlo simulations predict a structural stability diagram that contains domains of stability of an open honeycomb network, a compact phase, and a high-temperature disordered phase. The results are in agreement with recent experiments, and reveal a relationship between the molecular size and the network stability, which may be used to predict an upper limit on pore-cavity sizes.

DOI: [10.1103/PhysRevLett.100.156101](https://doi.org/10.1103/PhysRevLett.100.156101)

PACS numbers: 81.16.Dn, 05.10.Ln, 81.07.Nb

Open molecular networks on surfaces may serve as scaffolds for generating nanostructures [1–14], thus expanding the capabilities of bottom-up nanotechnology beyond self-assembly [15]. These nanostructures can be used in molecular photovoltaics [16], electrochemistry [17], medicine and biomaterials [18], and quantum information processing [19]. The molecular networks on surfaces are usually built from large molecules, which are coupled via highly directional forces, such as hydrogen bonding. In some cases less directional forces like van der Waals can trigger a network formation, in which the directionality of the interaction is due to the molecule geometry [20]. With its high selectivity and directionality [21], hydrogen bonding enables equilibrium molecular configurations to be achieved at relatively low processing temperatures [6,11,22,23].

The network morphology can be varied by using binary molecular mixtures with different molecular binding rules [24,25]. van der Waals interactions may interfere with these binding rules, decreasing the degree of directionality or the anisotropy of the molecular coupling. For large enough molecules van der Waals interactions can be comparable with or even exceed hydrogen-bond energies [26]. Therefore the network-forming molecules must be chosen such that the influence of van der Waals interactions is minimized. We make the first step towards defining the requirements for network-forming molecules by demonstrating the critical role played by the ratio of the van der Waals coupling energy to the hydrogen-bonding energy.

We choose a model system that possesses the characteristic features of a melamine-PTCDI molecular mixture [6,11,13–22] with its hydrogen bonding and van der Waals interactions and little influence from the underlying Au(111) or Si(111)-Ag substrates [11,27]. Hexagonal supramolecular networks were prepared in

UHV (10^{-8} Pa) by first outgassing a Si(111) sample ($3\text{ mm} \times 7\text{ mm}$) at $\sim 600^\circ\text{C}$ and flash annealing at 1200°C to form the Si(111)-(7 \times 7) reconstruction [6]. The Ag/Si(111)-($\sqrt{3} \times \sqrt{3}R30^\circ$) reconstruction was prepared by subliming Ag onto the surface at 550°C . PTCDI and melamine were sequentially deposited and the sample was then annealed at $\sim 80^\circ\text{C}$. Images were acquired using a commercial scanning tunnelling microscope (JSTM-4500S) using electrochemically etched *W* tips and operated under room temperature conditions.

Our model system assumes a fixed number of molecules confined in a sufficiently large area of a hexagonal grid corresponding to vacuum annealing of molecular mixtures on a surface. The way we combine directional and van der Waals bonding is illustrated in Fig. 1(a). The molecule at the center “0” is surrounded by six first nearest-neighbor sites on the hexagonal grid labeled 1 to 6. Some of these sites (1, 2, 3, 4, 6) are occupied by other molecules. Hydrogen bonds form between suitable functional groups, such as the pairs 0–1, 0–4, and 2–3. All nearest-neighbor molecules interact via van der Waals forces.

The interaction energy between two nearest-neighbor molecules of types μ and ν thus depends on their orientation. Let θ_μ (or θ_ν) represent the smallest of the angles that the hydrogen bond-generating functional group of molecule μ (or molecule ν) make with the bond direction from μ (ν) to ν (μ). Then the interaction energy between the nearest-neighbor molecules μ and ν is given by

$$E_{\mu\nu}(\theta_\mu, \theta_\nu) = E_{\mu\nu}^A(\theta_\mu, \theta_\nu) + E_{\mu\nu}^I \quad (1)$$

where $E_{\mu\nu}^I$ is the isotropic van der Waals interaction energy, and $E_{\mu\nu}^A(\theta_\mu, \theta_\nu)$ is the anisotropic, or directional, bonding energy that takes the values

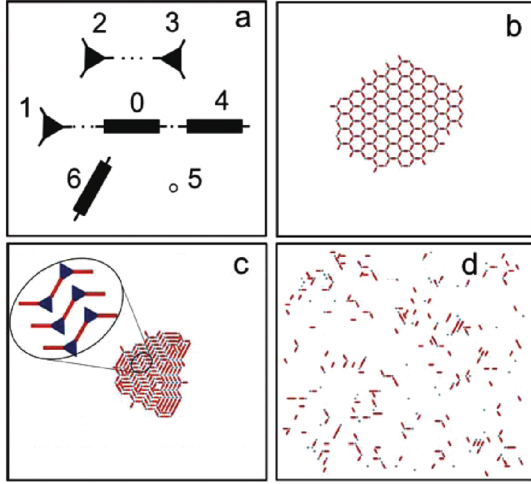


FIG. 1 (color). (a) Molecules on hexagonal grid illustrating anisotropic (hydrogen bonds) molecular bonding. Rodlike (PTCDI) molecules are shown as elongated rectangles, while vertexlike (melamine) molecules are triangles. Hydrogen-bond-generating functional groups are indicated by line segments; hydrogen bonds are shown by dotted line segments. (b)–(d) Phases of stoichiometric mixture of 180 rodlike and 120 vertexlike molecules observed in different regions of parameter space during KMC simulations: (b) network structure at $E^I = 0$ eV and $T = 0.08$ eV; (c) compact structure at $E^I = -0.16$ eV and $T = 0.1$ eV; magnified is main structural unit; (d) disordered structure at $E^I = -0.1$ eV and $T = 0.24$ eV.

$$E_{\mu\nu}^A(\theta_\mu, \theta_\nu) = \begin{cases} E_{\mu\nu}^A & \text{for } \theta_\mu = \theta_\nu = 0, \\ 0 & \text{otherwise.} \end{cases} \quad (2)$$

The anisotropic energies $E_{\mu\nu}^A$ in our model are taken to be the hydrogen-bonding energies corresponding to the formation of the hexagonal open network [28]: $E_{12}^A = -0.74$ eV (melamine-PTCDI), $E_{11}^A = -0.43$ eV (melamine-melamine), and $E_{22}^A = -0.5$ eV (PTCDI-PTCDI). Additional weaker hydrogen bonds could lead to more complicated molecular configurations, but we neglect this to keep the model simple. We assume that the isotropic interaction energy $E_{\mu\nu}^I$ is independent of species, so that $E_{\mu\nu}^I = E^I$, which we take as a variable parameter. Kinetic Monte Carlo (KMC) simulations [29] of the $\{N, V, T\}$ ensemble were used to study the structural stability diagram of a model system represented by a binary mixture of anisotropic molecules of type 1 (trigonal vertices, melamine) and type 2 (linear rods, PTCDI) occupying sites on a two-dimensional hexagonal lattice. The KMC technique is more computationally efficient than molecular dynamics as it does not follow the details of specific molecular trajectories, thereby significantly increasing the accessible time scale. Molecular vertices and rods can establish anisotropic bonding with three and two properly oriented nearest neighbors, respectively, so that the stoichiometric molecular mixture of 3 rods to 2 vertices can be arranged in a perfect honeycomb structure. In two

dimensions the influence of the surface on the energetics decreases as $1/\sqrt{N_m}$, where N_m is the total number of molecules in a system. Therefore, we have chosen the system size to be large enough to represent a macroscopic molecular cluster within a few-percent accuracy in the structural stability diagram shown in Fig. 2. This corresponds to a stoichiometric system with 120 vertices and 180 rods distributed over a 60×60 hexagonal lattice.

The equilibrium structure of the model system depends on the parameters $E_{\mu\nu}^A$, E^I , and the temperature T , and can be an open network (b), a close-packed or compact phase (c), or a disordered phase (d), as shown in Fig. 1. Each of these structures can be characterized by an average coupling energy per molecule $\bar{\epsilon}$ and the mean molecular coordination number $\bar{\eta}$. The network structure shown in Fig. 1(b) is stable at low temperatures and low values of E^I . A corresponding infinite defect-free system at $T = 0$ would be characterized by saturated hydrogen bonds with molecular energy $\bar{\epsilon}_n = \frac{6}{5}(E_{12}^A + E^I)$ and coordination number $\bar{\eta}_n = 2.4$. In contrast, an infinite compact structure at $T = 0$ is characterized by full coordination $\bar{\eta}_c = 6$ with a molecular energy $\bar{\epsilon}_c = \frac{1}{5}(4E_{12}^A + E_{22}^A) + 3E^I$. This energy can be determined simply from the characteristic building block of this structure, which is enlarged in Fig. 1(c). The compact structure becomes stable for $\bar{\epsilon}_c < \bar{\epsilon}_n$ which occurs for $E^I < 0.22E_{12}^A - 0.11E_{22}^A \approx -0.11$ eV corresponding to $E^I/E_{12}^A > 0.14$. The disordered structure shown in Fig. 1(d) has both the lowest coupling energy and

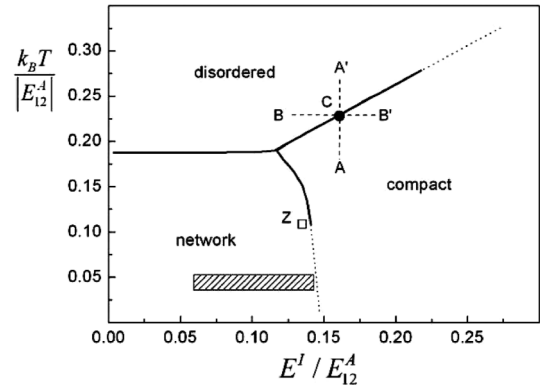


FIG. 2. Structural stability diagram of system shown in Fig. 1 in parameter space of normalized temperature $k_B T / E_{12}^A$ versus ratio of isotropic (van der Waals) to anisotropic (hydrogen-bond) energies E^I / E_{12}^A . Solid curves indicate structural transitions between three domains identified as network, close-packed or compact, and disordered phases. Shaded region indicates likely region of parameters corresponding to melamine-PTCDI molecular system. Lines AA' and BB' indicate directions for obtaining heat capacity C_V and generalized susceptibility χ_E in Fig. 3. The open square symbol at $k_B T / E_{12}^A = -0.108$ and $E^I / E_{12}^A = 0.135$ indicates parameters of simulated system displayed in Fig. 4. We use elevated temperatures in our simulations to reach equilibration within a reasonable time. Therefore structural defects are also more likely to be observed.

the lowest mean coordination number, and exists only at higher temperatures due to entropic effects.

The boundaries between different structures are found by analyzing the heat capacity at constant volume C_V and the generalized susceptibility χ_E , defined as a partial derivative of the coordination number with respect to the van der Waals energy E^I , that is considered as an external variable.

The heat capacity C_V is calculated from the energy fluctuations $\langle \delta E^2 \rangle = \langle E^2 \rangle - \langle E \rangle^2$ [29],

$$C_V = (\langle E^2 \rangle - \langle E \rangle^2) / (k_B T^2), \quad (3)$$

where $\langle \dots \rangle$ is the statistical average over the microstates adopted by the system in equilibrium, and k_B is the Boltzmann constant. In order to obtain the generalized susceptibility $\chi_E = \partial \langle X \rangle / \partial |E^I|$ we first identify the corresponding conjugate variable X such that the system energy would be proportional to $X \cdot E^I$. The energy of a system containing N_m molecules in a bonding configuration Σ is given by

$$E_\Sigma = -\frac{1}{2} N_m \bar{\eta} |E^I| + \frac{1}{2} \sum_{i,j} n_{ij} E_{ij}^A, \quad \text{where} \quad \bar{\eta} = \frac{1}{N_m} \sum_{i=1}^{N_m} \eta_i. \quad (4)$$

We see that the mean molecular coordination number $\bar{\eta}$ can be considered as a variable conjugate to E^I . The sum in Eq. (4) takes into account hydrogen-bond contributions, which are proportional to the numbers n_{ij} of hydrogen-bond couplings between the molecular types i and j . The generalized susceptibility is now obtained using a statistical mechanics definitions of the average value and variance of $\bar{\eta}$,

$$\langle \bar{\eta} \rangle = \sum_{\Sigma} \bar{\eta} \exp(-E_\Sigma / (k_B T)) / Z,$$

$$\text{where} \quad Z = \sum_{\Sigma} \exp(-E_\Sigma / (k_B T)) \quad (5)$$

$$\begin{aligned} \langle \delta \bar{\eta}^2 \rangle &= \langle \bar{\eta}^2 \rangle - \langle \bar{\eta} \rangle^2 = (2k_B T / N_m) \partial \langle \bar{\eta} \rangle / \partial |E^I| \\ &= (2k_B T / N_m) \chi_E. \end{aligned}$$

Hence

$$\chi_E = (N_m / 2k_B T) (\langle \bar{\eta}^2 \rangle - \langle \bar{\eta} \rangle^2). \quad (6)$$

A structural stability diagram for the model system is presented in Fig. 2. The normalized axes are temperature $\tilde{T} = k_B T / E_{12}^A$ and isotropic coupling energy $\tilde{E}^I = E^I / E_{12}^A$. In particular, a domain boundary is indicated by a divergence (or maximum in our finite system) of C_V and/or χ_E as a function of T and E^I , respectively, which according to Eqs. (5) and (6) can be related to the average variance of the system energy and the mean molecular coordination number, respectively. In Fig. 3 we illustrate the heat capacity C_V with varying system temperature along the line AA' in Fig. 2 and the susceptibility χ_E with varying E^I

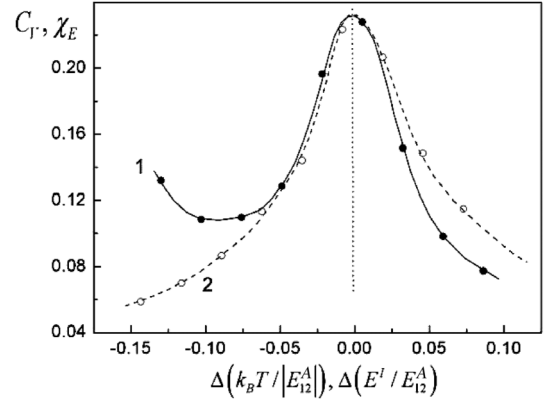


FIG. 3. Heat capacity C_V (curve 1) and generalized susceptibility χ_E (curve 2) of system in Fig. 1 indicating structural transition between compact and disordered phases at point C in Fig. 2 with coordinates $k_B T / E_{12}^A = -0.16$ and $E^I / E_{12}^A = 0.11$. Functions are scaled to have the same peak value. The origin of the curve is in both cases at the maximum of the function.

along the line BB'. Both curves show peaks at the same position indicating one and the same structural transformation between the compact and disordered phases, which takes place at the point C in Fig. 2. The full structural stability diagram is obtained by connecting all similar structural transition points in the (\tilde{T}, \tilde{E}^I) space, and is shown in Fig. 2 by the solid lines. By investigating the system size dependence of our structural stability diagram we found that it deviates by only few percent from its asymptotic shape in an infinite system. We can, therefore, extrapolate our predicted structural transition line at finite temperatures to the transition point at zero temperature, which we calculated for an infinite system. The theoretical structural stability diagram is scale invariant; simultaneous scaling of all interaction energies and temperature leaves the diagram unchanged.

The shaded area in Fig. 2 indicates the experimental conditions for fabricating the melamine-PTCDI networks [6,22]. It takes into account processing temperatures $T \approx 60^\circ\text{--}80^\circ\text{C}$ and a likely range of van der Waals interaction energies. The latter is estimated to be of the order of the coupling energies for benzene dimers [26] while not exceeding the stability values for the network structure, i.e., within the range $\sim 0.04\text{--}0.1$ eV. According to this estimate the melamine-PTCDI network energy is close to that of the compact phase suggesting that the clusters of the compact structure may appear within the network. Recently we have experimentally observed such clusters inside the network structure [Fig. 4(a)] that show similarity to the predictions of the model [Fig. 4(b)]. However, a detailed analysis reveals that the simulated and experimentally observed compact structures are not identical, which is possibly due to the extra hydrogen bonding illustrated in Fig. 4. Further investigations are required to identify this extra bonding and to elaborate a more sophisticated model.

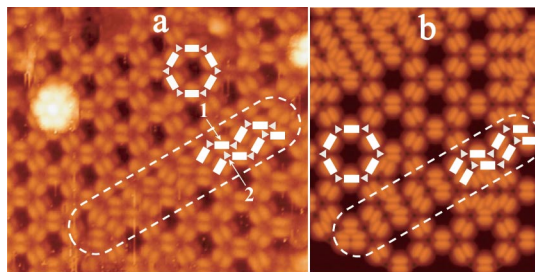


FIG. 4 (color). PTCDI-melamine molecular structures with PTCDI molecules appearing as bright double lines and melamine molecules not resolved. (a) STM image of on the Ag/Si(111)-($\sqrt{3} \times \sqrt{3}R30^\circ$) surface at room temperature; (b) simulated structure obtained for the parameter values corresponding to the open square symbol in Fig. 2. White bars indicate the positions of PTCDI molecules and white triangles those of the melamine molecules. Hexagons in both (a) and (b) represent structural unit of the equilibrium structures, while the clusters of the compacted structures outlined by white dashed lines represent typical defects. The compact structures in (a) and (b) are not identical, as illustrated by white symbols inside outlined areas. However, they consist of the same zigzag motif with a different side shift that is likely to be stabilized by an additional hydrogen bond between PTCDI (1) and melamine (2), as labeled in (a).

In the structural stability diagram in Fig. 2, the network structure is stable for all temperatures in the shaded experimental region for $E_{12}^A/E^I \geq 8$. This sets a lower limit for the hydrogen-bonding energy E_{12}^A between the molecules to form the open hydrogen-bonded network if the van der Waals energy E^I remains unchanged. A decreased strength of the hydrogen bonding would yield a spread of the shaded area in Fig. 2 into the compact-structure domain. This effect may be responsible for an easier formation of more compact phases in the PTCDA-melamine system [11], where the vertex-rod bonding is $E_{12}^A = -0.13$ eV. We would anticipate difficulties in forming open networks with larger molecules, since the van der Waals force scales with size [26]. This sets an upper size limit of about 7 nm for rodlike molecules if the hydrogen-bonding strength is the same as in the PTCDI-melamine system. The simulations also suggest an alternative route for stabilizing supramolecular networks through the reduction of the van der Waals interaction by attaching bulky side groups which inhibit the formation of regular close-packed phases.

Our results reveal a fundamental constraint on the ratio between the directional and isotropic coupling energies for the molecules to form stable surface network structures or templates. Breaking this constraint leads to network collapse, as is predicted by our simulations and observed in

experiments on PTCDA-melamine systems [11]. This will provide an additional guideline in helping the design of molecular mixtures with improved self-assembling properties.

We thank B. L. Rogers for calculating hydrogen-bond energies in the melamine-PTCDI molecular system, and R. Drautz and F. Silly for discussions. We thank EPSRC for the collaborative project “supramolecular self-assembly of 1–10 nm templates for biofunctional surfaces, quantum information processing and nanoelectronics” (No. EP/D048761/1). G. A. D. B. thanks EPSRC for financial support (No. GR/S15808/01).

-
- [1] M. Böhringer *et al.*, Phys. Rev. Lett. **83**, 324 (1999).
 - [2] J. V. Barth *et al.*, Angew. Chem., Int. Ed. **39**, 1230 (2000).
 - [3] M. Furukawa, H. Tanaka, and T. Kawai, Surf. Sci. **445**, 1 (2000).
 - [4] S. Griessl *et al.*, Single Mol. **3**, 25 (2002).
 - [5] D. L. Keeling, Nano Lett. **3**, 9 (2003).
 - [6] J. A. Theobald *et al.*, Nature (London) **424**, 1029 (2003).
 - [7] Q. Chen, D. J. Frankel, and N. V. Richardson, Langmuir **18**, 3219 (2002).
 - [8] A. Dmitriev *et al.*, J. Phys. Chem. B **106**, 6907 (2002).
 - [9] H.-J. Yan *et al.*, J. Phys. Chem. B **108**, 11 251 (2004).
 - [10] S. Clair *et al.*, J. Phys. Chem. B **108**, 14 585 (2004).
 - [11] J. S. Swabrick *et al.*, J. Phys. Chem. B **109**, 12 167 (2005).
 - [12] R. Otero *et al.*, Angew. Chem., Int. Ed. **44**, 2270 (2005).
 - [13] L. M. A. Perdigão, N. R. Champness, and P. H. Beton, Chem. Commun. (Cambridge) **5**, 538 (2006).
 - [14] L. M. A. Perdigão *et al.*, Phys. Rev. B **73**, 195423 (2006).
 - [15] J. C. Huie, Smart Mater. Struct. **12**, 264 (2003).
 - [16] M. S. Kang *et al.*, J. Power Sources **160**, 711 (2006).
 - [17] S. P. Jiang *et al.*, Electrochem. Solid State Lett. **8**, A574 (2005).
 - [18] A. Firth *et al.*, Nanomedicine **1**, 189 (2006).
 - [19] J. J. L. Morton *et al.*, Nature Phys. **2**, 40 (2006).
 - [20] K. Tahara *et al.*, J. Am. Chem. Soc. **128**, 16 613 (2006).
 - [21] G. A. Jeffrey, *An Introduction to Hydrogen Bonding* (Oxford University Press, New York, 1997).
 - [22] L. M. A. Perdigão *et al.*, J. Phys. Chem. B **110**, 12 539 (2006).
 - [23] J. S. Swabrick *et al.*, J. Phys. Chem. B **110**, 6110 (2006).
 - [24] R. E. A. Kelly and L. N. Kantorovich, Surf. Sci. **589**, 139 (2005).
 - [25] R. E. A. Kelly, Y. J. Lee, and L. N. Kantorovich, J. Phys. Chem. **109**, 11 933 (2005).
 - [26] S. Grimme, J. Comput. Chem. **25**, 1463 (2004).
 - [27] S. K. M. Henze *et al.*, Surf. Sci. **601**, 1566 (2007).
 - [28] J. Ma *et al.*, J. Phys. Chem. B **110**, 12 207 (2006).
 - [29] M. E. Newman and G. T. Barkema, *Monte Carlo Methods in Statistical Physics* (Clarendon Press, Oxford, 1999).